

Reversible Emission Tunability from 2D-Layered Perovskites with Conjugated Organic Cations

Balaji Dhanabalan, Renuka D. Pothuraju, Sergio Marras, Lea Pasquale, Liberato Manna, Roman Krahne,* and Milena P. Arciniegas*

The structural flexibility of 2D-layered halide perovskites provides unprecedented opportunities for tuning their optical properties. For example, lattice distortions facilitate white emission that stems from self-trapped excitons or defects, and organic cations and halides determine structural stability and emission range. Herein, the optical properties of a set of single-layer thiophene-based 2D lead bromide platelets are investigated. Blue- and white-emitting materials based on the choice of thiophene cation and HBr concentration in the synthesis and reversible white to blue color switching by sequential washing and precursor exposure of the fabricated samples are obtained. The photophysical and structural studies indicate that the key to color switching is the formation and suppression of self-trapped excitons by the supply and removal of cations and halides in acetone. The range of emission color from these materials is extended to red by efficient Mn doping that leads to an additional strong emission peak centered at 620 nm. The findings stimulate the development of color-tunable and switchable light emitters based on a single material.

1. Introduction

2D hybrid layered perovskites (2D HLPs) are extremely versatile materials in view of their outstanding defect tolerance, which allows an ample choice of combinations of organic and inorganic building blocks.^[1,2] To date, the Ruddlesden–Popper structures made of organic layers built by pairs of monovalent cations separating inorganic layers are among the most studied ones.^[3,4] They manifest a Van der Waals gap between interdigitated organic cations, and the next-neighbor inorganic layers are

half-cell shifted.^[5] Compared with the 3D perovskite family, the large organic cations used in 2D HLPs made them highly stable against the environment.^[6] This property has been transferred to optoelectronic devices by combining 2D HLPs with 3D perovskites.^[7] Moreover, the alternated architecture of organic/inorganic layers in these materials confers quantum and dielectric confinement effects to them, in addition to their large exciton binding energies and lifetimes and strong spin–orbit coupling.^[8] Because of these properties, 2D HLPs are potential materials for light-emitting applications, spintronics, and flexoelectronics.^[4,9] A key advantage of 2D HLPs is that they can also be fabricated by quick, simple, and low-cost strategies.^[10,11]

One fascinating property of 2D HLPs is their broadband emission at room temperature (RT).^[12,13] These structures can be seen as potential single-source emitters of white light, with desired color chromatic coordinates and excellent color rendering index (CRI).^[14,15] The broadband emission is typically attributed to elastic distortions of the lattice caused by strongly bound excitons,^[16] although recent reports have shown that the broadband emission can be also generated from structural defects, such as halide interstitials or organic vacancies that act as color centers.^[17,18] Most of the examples of broadband-emitting 2D HLPs come from corrugated structures, that is, (110)-oriented crystals commonly synthesized with relatively complex organic cations, and their accommodation induces strong distortions to the inorganic layers.^[1,19] Examples of such organic cations are, among others, 2,2'-(ethylenedioxy)bis(ethylammonium),^[20] N-(3-aminopropyl)imidazole,^[21] 2-(aminoethyl)isothiourea,^[22] and 2-(dimethylamino)ethylamine.^[23] In the case of (100)-layer orientation, the broadband emission at RT is observed only in a few cases^[17,18,24] and was explained in terms of structural defects. Frequently reported cations, such as phenethyl- and butylammonium, typically produce a narrow blue emission. Overall, these studies highlight the degree of freedom of 2D HLPs to control their properties through structural engineering. However, because of the large variety of organic molecules that, in principle, can be used to build these materials, only a very small fraction has been explored, which is mostly based on electrically isolating organic layers. Here, we show the reversible emission tunability, from white to blue to white, of Ruddlesden–Popper 2D HLPs that are synthesized with thiophene cations by

B. Dhanabalan, R. D. Pothuraju, S. Marras, Dr. L. Pasquale, Prof. L. Manna, Prof. R. Krahne, Dr. M. P. Arciniegas
Istituto Italiano di Tecnologia
Via Morego 30, 16163 Genova, Italy
E-mail: Roman.Krahne@iit.it; Milena.Arciniegas@iit.it

B. Dhanabalan, R. D. Pothuraju
Dipartimento di Chimica e Chimica Industriale
Università degli Studi di Genova
Via Dodecaneso, 31, 16146 Genova, Italy

 The ORCID identification number(s) for the author(s) of this article can be found under <https://doi.org/10.1002/adpr.202100005>.

© 2021 The Authors. Advanced Photonics Research published by Wiley-VCH GmbH. This is an open access article under the terms of the Creative Commons Attribution License, which permits use, distribution and reproduction in any medium, provided the original work is properly cited.

DOI: 10.1002/adpr.202100005

controlling their chemical composition. These cations are part of the π -conjugated molecule family, for which significantly improved charge mobility in 2D HLP-based solar cells has been recently demonstrated.^[25] Furthermore, we show how such thiophene-based 2D HLPs can be easily doped to generate dual emission from a single structure. Given the importance of these materials for light-emitting applications, the strategies to modulate their photoluminescence (PL) as desired are highly appealing, in particular, because these properties come together with enhanced organic–inorganic charge transfer features that are inherent to thiophenes.

2. Results and Discussion

The preparation of the thiophene-based 2D lead bromide LP was conducted by following our simple synthesis protocol, with slight modifications.^[10] We focused on two thiophene molecules, 2-thiophenemethylammonium (TMA) and 2-thiopheneethylammonium (TEA), and investigated the role of the cation and halide content on the photophysical characteristics of the resulting structures. The difference between these two organic cations resides on the shorter length of the carbon chain that links the NH_3 group and the aromatic ring containing the S atom. For the synthesis, PbBr_2 and HBr were dissolved in acetone to form a transparent solution. The selected thiophene was injected into the mixture, triggering within few seconds the formation of crystals in the solution (the solvent used here was

either acetone or toluene). Then, the crystals were washed twice with acetone and stored at RT for further studies (see the Experimental Section for details). We fabricated both TEA and TMA samples using different precursor concentrations for thiophenes and HBr, namely, 0.6 mmol and 1.2 mmol (see Experimental Section for details). From here we name the as-synthesized samples using the concentration of the thiophene and HBr precursors used in the synthesis followed by abbreviation of the organic cation. **Figure 1a–b** shows the collected scanning electron microscopy (SEM) images from the as-synthesized crystals prepared with a high concentration (1.2 mmol) of the selected thiophene cation and HBr. The sketches on the left side of the figures display the structure of the organic molecule used in the synthesis. All the 2D HLP crystals have a platelet-like morphology with lateral size of about $50\ \mu\text{m}$ (see a larger set of SEM images in Figure S1, Supporting Information). From the 1.2 mmol TMA sample (Figure 1b), elongated structures can also be observed, which resemble the morphology of 1D-layered structures.^[26] Our powder X-ray diffraction patterns however confirm that all the samples are made dominantly by alternated organic/inorganic periodic layers with corner-sharing Pb–Br octahedra, that is, a 2D configuration. From the experimental powder XRD patterns in Figure 1c–d, we observe periodic reflections from which the interdistances, d , between Pb–Br layers were estimated as 15.75 and 14.49 Å for TEA- and TMA-based crystals, respectively, regardless of the cation content. We used as a reference the reported crystallographic data for $(\text{TMA})_2\text{PbI}_4$ ^[25] after

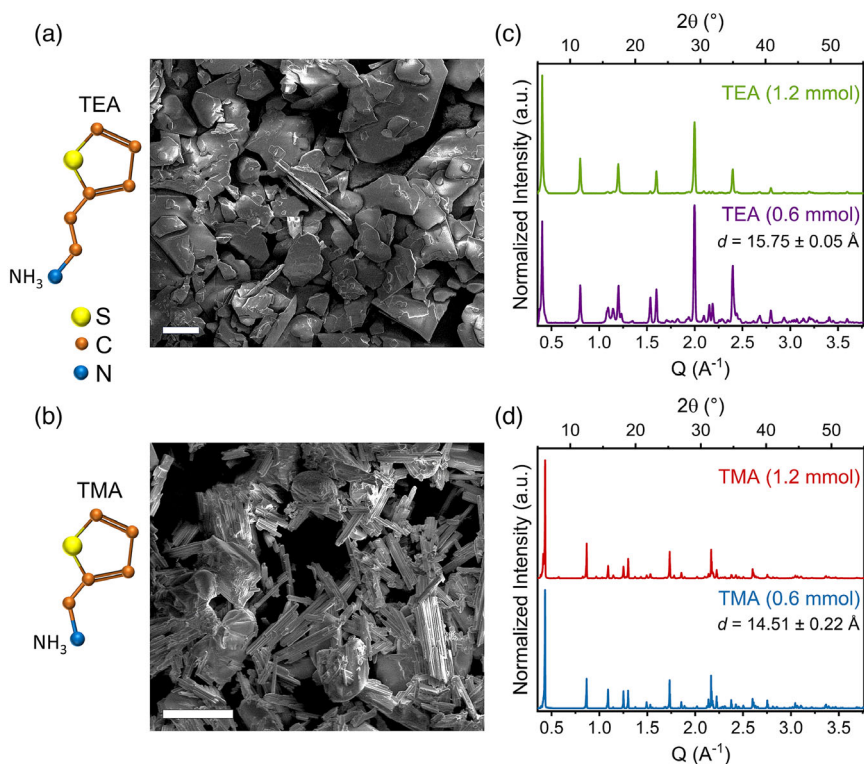


Figure 1. a,b) SEM images showing the morphology of the as-synthesized crystals prepared using conjugated organic cations, a) 2-thiopheneethylamine (TEA) and b) 2-thiophenemethylamine (TMA), as represented in the sketches. Scale bars: $50\ \mu\text{m}$. c–d) Powder XRD patterns collected from the crystals prepared with different concentrations of HBr and amines. The interdistance between inorganic Pb–Br layers, d , is indicated in the panels.

substituting I^- halide anions for Br^- ones in the structure (Figure S2, Supporting Information) and refining the cell parameters using CrystalDiffract v. 6.9.0 software.^[27]

We notice that while the length of the cell unit in the c direction remained unchanged ($\approx 29.0 \text{ \AA}$), there is a contraction in both a and b in-plane cell parameters. The relative intensities of the peaks in the XRD patterns are affected by preferential orientation of the 2D HLP platelets, in particular for the TEA samples. Overall, we confirm good matching between the different angular positions and number of diffraction peaks observed on the experimental patterns with those in the simulated one (Figure S2, Supporting Information), which indicates that these structures share the same crystallographic lattice, that is, an orthorhombic cell unit with the $pbca(61)$ space group.

Figure 2a-b shows photographs of the crystals under ultraviolet (UV) light. While the TEA samples both show deep-blue emission, there is strong change on the emission of TMA, from blue to white, when the cation and halide content during synthesis increases. Table S1, Supporting Information, shows the optical characteristics at RT of the synthesized samples.

Upon excitation with a laser at 375 nm wavelength, the TEA samples display deep-blue emission with a double-peak structure (414–425 nm) that is characteristic of ensembles of 2D HLPs.^[10,25,28] This blue band edge emission is accompanied by weak broadband emission in the green–red spectral range that is more pronounced in the 0.6 mmol TEA sample (as shown in the inset in Figure 2c). The TMA samples also show the blue

band edge emission, although here the double peak feature is less resolved. Furthermore, the peak maximum of the 1.2 mmol TMA sample is slightly red shifted with respect to the 0.6 mmol one, and the blue peak is overall broader. Concerning the broad emission and concentration of amine and Br precursors, the TMA sample behaves opposite to the TEA sample. For TMA, the broad emission peak is stronger for the 1.2 mmol sample with respect to the 0.6 mmol one (Figure 2d). Also, the broad emission peak is much more dominant with a maximum amplitude (centered at $\approx 520 \text{ nm}$) almost equal to the blue band edge emission, with full width half maximum (FWHM) of about 190 nm (corresponding to $\approx 810 \text{ meV}$). For all the samples, the absorption spectra (dotted lines in Figure 2c-d) show band edges in the region from 380 to 430 nm, with slight differences in their excitonic peaks. For TEA, we observe a double-peak structure at the band edge that we attribute to confined excitons,^[10,29] which corresponds well to the double peak observed in the emission spectra. The double-peak feature is sharper and more developed for the 1.2 mmol TEA sample, pointing to a more regular and defect-free crystal structure. While for both TMA samples the absorption onset occurs at roughly the same wavelength (around 430 nm), the peaks in the absorption spectra above the onset are very different. For the 0.6 mmol TMA sample, a double-peak structure is present, similar to the TEA samples, but for the 1.2 mmol TMA sample, a broader peak at a much shorter wavelength (365 nm) is observed. To get more insight into the photophysics underlying the emission, we conducted

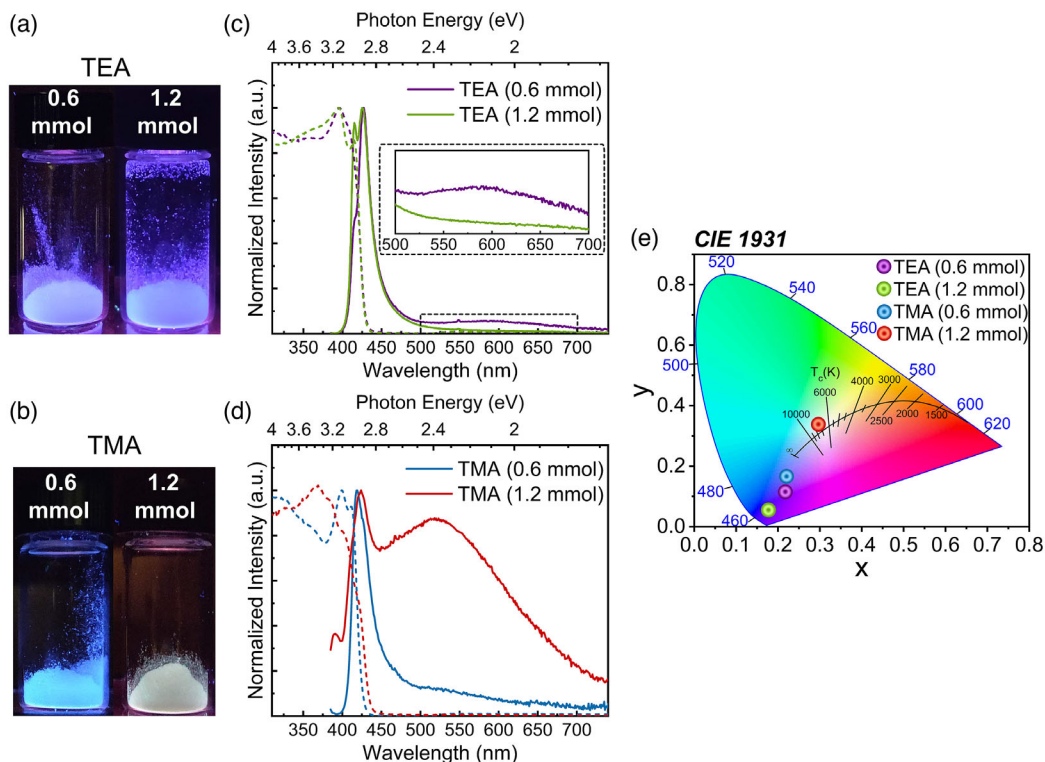


Figure 2. a,b) Photographs of the vials containing the a) TEA- and b) TMA-based dried crystals under UV light. c,d) Emission (solid lines) and absorption (dashed lines) spectra collected from the samples prepared with different conjugated organic cations at low (0.6 mmol) and high (1.2 mmol) precursor concentrations. e) CIE chromaticity coordinates of the crystals showing from deep-blue to cold white emission depending on the concentration of the conjugated organic cations used in their synthesis.

photoluminescence excitation (PLE) spectra with detection bands centered at the maxima of the emission peaks, in particular at the maxima of the broadband emission. The results are shown in Figure S3, Supporting Information, and show a very different behavior for the TMA samples fabricated with low and high precursor concentrations. For the 0.6 mmol TMA sample, the lowest-energy PLE peak is red shifted with respect to the absorption spectrum, whereas for the high-concentration sample, it is blue shifted. In the former case that means that the broad emission can be excited by pumping into the Stokes-shifted energy levels of the emitting states (corresponding to the optical pumping of defects), whereas in the latter the broadband emission requires pumping above the band edge. Similar to the 0.6 mmol TMA sample, the broad emission from the 0.6 mmol TEA sample can be excited by pumping the emitting states. This points to a different emission mechanism for the prominent broad emission observed from the 1.2 mmol TMA sample with respect to that of the samples obtained with low precursor concentration. The behavior of the 1.2 mmol TMA sample is in agreement with the self-trapped exciton (STE) emission mechanism that requires the trapping of excitons that were excited above the band edge,^[30] and this interpretation is further supported by the observation of STE in (100)-oriented 2D Ruddlesden–Popper perovskites.^[24,31] Also concerning the effect of the higher concentration of the organic cations and HBr in the synthesis, the TMA sample behaves differently from the TEA one. For the TEA sample, the broad emission is suppressed when using a higher cation and HBr concentration (see inset in Figure 2c), which points to broad emission from organic and halide vacancies^[17] that are more efficiently passivated when using higher TEA and

HBr concentrations. For the TMA sample, the broad emission is obtained using higher organoamine and Br precursor concentrations in the synthesis. Here in principle, Br atoms can occupy interstitial positions at the inorganic layer that can induce the broad emission.^[32] However, if we only increase the concentration of HBr in the synthesis (that is, the TMA concentration is 0.6 mmol and the HBr one is 1.2 mmol), the broad peak is not present in the emission spectrum (Figure S4, Supporting Information), which indicates that such interstitials are not at the origin of the observed broadband emission. Therefore, we conclude that the broad emission of the 1.2 mmol TMA sample is intrinsic to its structure. These differences observed on the emission profiles of the samples are translated to their corresponding Commission Internationale de l’Eclairage (CIE) coordinates: the emission colors are located in the deep-blue region except for the 1.2 mmol TMA crystals that show close-to-pure white light with chromaticity coordinates of (0.33, 0.33) (Figure 2e).

To better understand the emission dynamics of the samples, we recorded the PL decay traces related to the blue band edge and broad emission peaks (Figure 3). The decay traces of the TEA samples are characterized by a fast and a slow component, τ_1 and τ_2 (for accurate fitting, a function with three exponential decays was needed; however, the weight of the third exponential was around 1% or less (see Table S2, Supporting Information)).

For the 0.6 mmol TEA sample, the τ_1 lifetime component of the blue emission is around 1 ns and has $\approx 90\%$ weight (τ_2 is around 2 ns with 8% weight), whereas for the broad emission τ_2 is 3.6 ns and has 23% of the weight. A higher precursor concentration here leads to the reduced weight of the fast component (from 90 to 75%) and a correspondingly increased weight

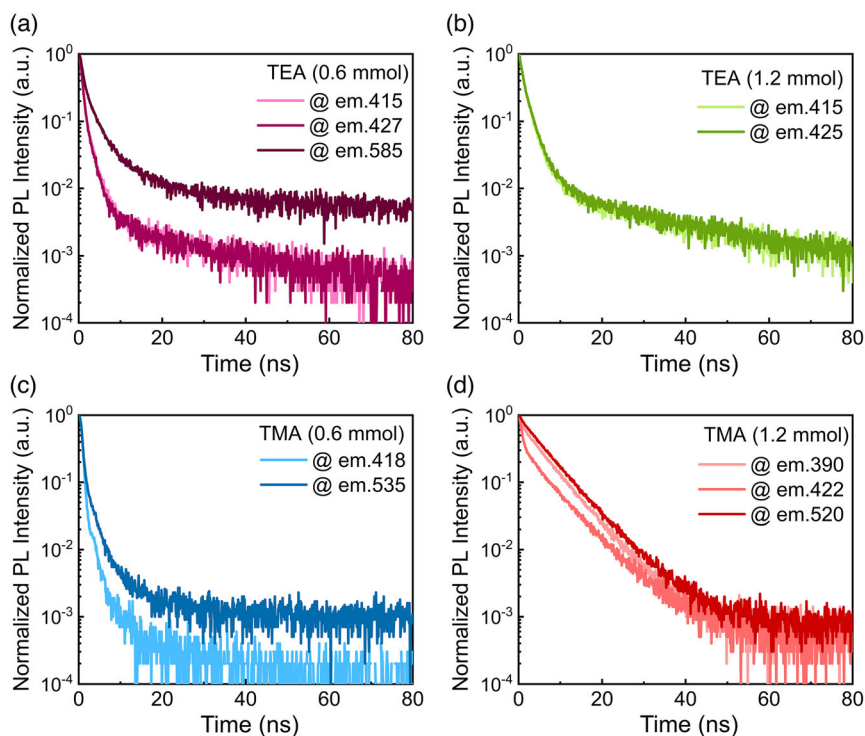


Figure 3. a-d) PL decay profiles acquired from the samples prepared using different concentrations of Br and the selected conjugated cation and collected at different wavelengths corresponding to their different emission peaks. The detection wavelength is given in nm in the legends in each panel.

(to around 25%) of the slow decay with lifetime of 2.6 ns for blue emission. As the fast component is typically associated with non-radiative decays caused by unpassivated defects, this behavior points to a more efficient defect passivation in the samples prepared with higher amine and HBr concentrations. Overall, the relatively strong contribution of a fast component associated with nonradiative decay is in agreement with the relatively low photoluminescence quantum efficiency (PLQE) of the samples that is around 2–3% (see Table S3, Supporting Information). The PL decay parameters of the 0.6 mmol TMA sample are similar to those of the 0.6 mmol TEA one, with slightly faster decay and less weight on the longer lifetime component. However, the 1.2 mmol TMA sample behaves very differently: the long lifetime component is around 6 ns and has a much higher weight (83% for the broad emission peak) in the decay. The overall similarity

of the PL decays probed at different emission wavelengths for the 1.2 mmol TMA sample (Figure 3 and S5c, Supporting Information) points to thermal equilibrium of the emitting states, as observed for other 2D-layered perovskite materials.^[13,33] Such behavior corroborates the interpretation in terms of self-trapped excitons. Concerning the similar PLQE for both TEA samples, the differences in the relaxation dynamics are most likely too small to produce a significant effect on the emission yield.

Interestingly, the emission of the TMA samples can be substantially modified by postsynthesis treatments like washing with acetone or exposing them again to precursor solutions. The reversible switching of the emission properties of the TMA sample is demonstrated by a series of photographs of the sample under UV light after subsequent treatments, as shown in **Figure 4**: the strong broadband emission from the 1.2 mmol

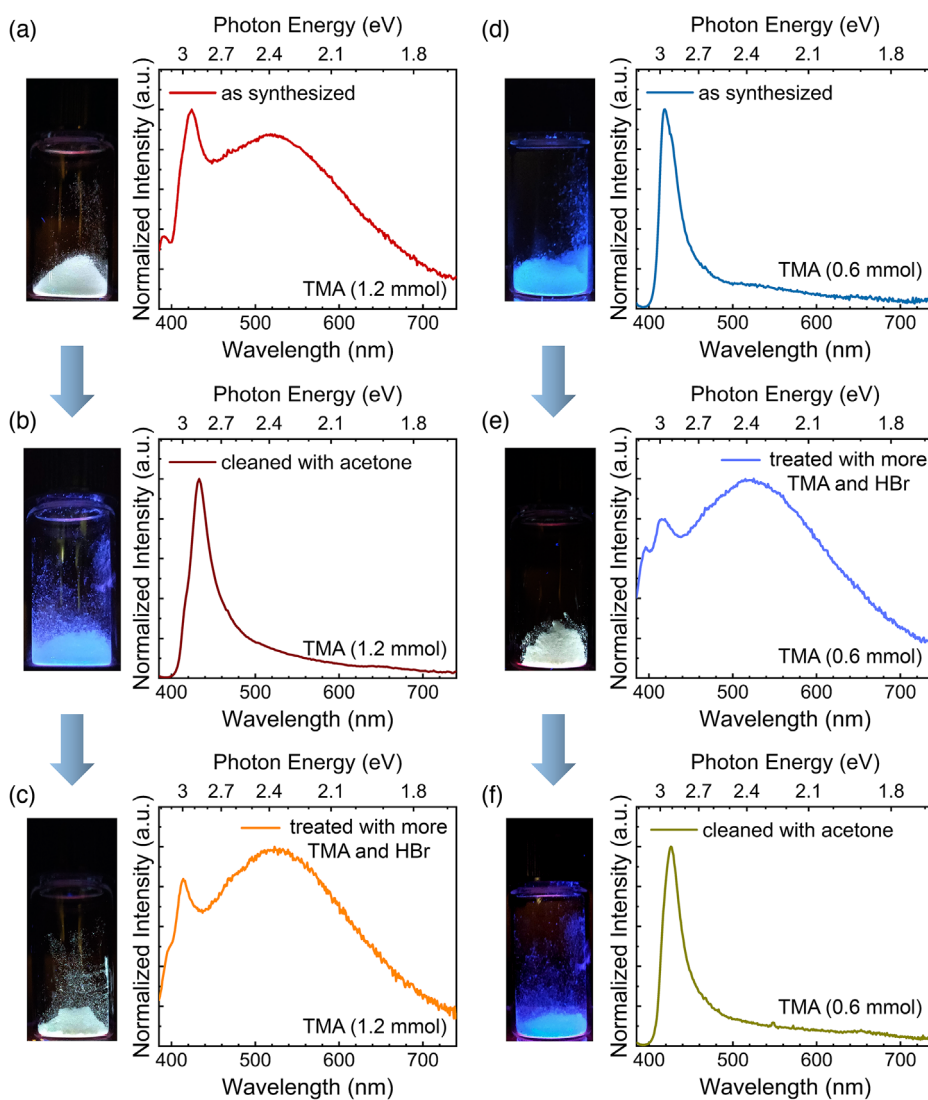


Figure 4. a–c) Emission spectra collected from the TMA-based crystals a) before and b) after different treatments conducted on the same 1.2 mmol TMA sample: b) washed several times with acetone showing only a blue emission peak with a long tail and c) after treatment with TMA-Br (in orange) that display the recovery of the broad emission. d–f) The broad emission can also be obtained by exposing the (low concentration) 0.6 mmol TMA sample to solutions with higher precursor concentrations in a reversible way. The photographs on the left side of the panels show the corresponding crystals under UV light exposure.

TMA sample (Figure 4a-c) is completely suppressed by washing the sample multiple times (6×) in acetone (Figure 4b). Then, it can be restored by exposing the platelets to the amine/Br precursor solutions, where both concentrations (0.6 and 1.2 mmol) have the same effect (Figure 4c, d-e).

One plausible explanation for this switching behavior is that the supply of TMA and Br triggers a transition to a more low-dimensional phase of the system, which is more distorted and sustains stronger broadband emission.^[34] Then, washing with acetone removes the excess organic moieties and restores the blue-emitting 2D phase. Furthermore, the acetone washing can lead to the absorption of acetone molecules at the organic vacancy positions, reducing the ability of such defects to trap electrons,^[14] which can reduce the broadband emission and favor the blue band-edge PL. This is not observed if the samples are washed with toluene (see Figure S6, Supporting Information). The XRD patterns collected from the white-emitting samples at different stages (Figure S6, Supporting Information) show the reappearance of a set of diffraction peaks with low intensity (thus after post-treatment with HBr and TMA in acetone), which supports our interpretation based on the formation of a more distorted subphase in the white-emitting samples. We note that color switching is not observed if the samples are washed with toluene (see Figure S6, Supporting Information).

The emission of the thiophene-based 2D HLPs can be further tuned by doping with Mn²⁺ ions, which has not been reported so far for layered structures made of conjugated cations.

The Mn-doped 2D HLPs bring interesting properties, such as highly Stokes-shifted emission, dual emission from a single material, and possibly enhanced magneto–optical and transport properties within the inorganic layer, as well as reduced electron–phonon-coupling.^[32] In thiophene-based 2D HLPs, the conjugated cations will additionally bring enhanced out-of-plane conductivity. We synthesized crystals using two different ratios of Pb:Mn precursors, 1:1 and 2:1, following the same protocol for the preparation of thiophene-based 2D HLPs and using a high content of cations and Br (1.2 mmol) (see details in Experimental Section). The samples were annealed to promote the incorporation of Mn ions into the structure. The results obtained via inductively coupled plasma–optical emission spectroscopy (ICP-OES) confirm the incorporation of Mn into the structures. The complete chemical compositions are shown in Table S4, Supporting Information. Mn, as other metal cations, can fully or partially replace Pb in the inorganic lattice or occupy interstitial positions.^[35,36] A substitution of the organic cation by Mn²⁺ will cause nonbalanced charges.^[37] Figure 5a,b shows the XRD patterns collected from the Mn-doped crystals.

We observe good agreement on the relative positions of the diffraction peaks of the Mn-doped samples with respect to the undoped ones, indicating that their periodic structure is preserved. Also, there is slight shift of the peaks towards higher 2θ angles, with respect to the undoped samples (see insets in Figure 5a–b and S7, Supporting Information), which indicates

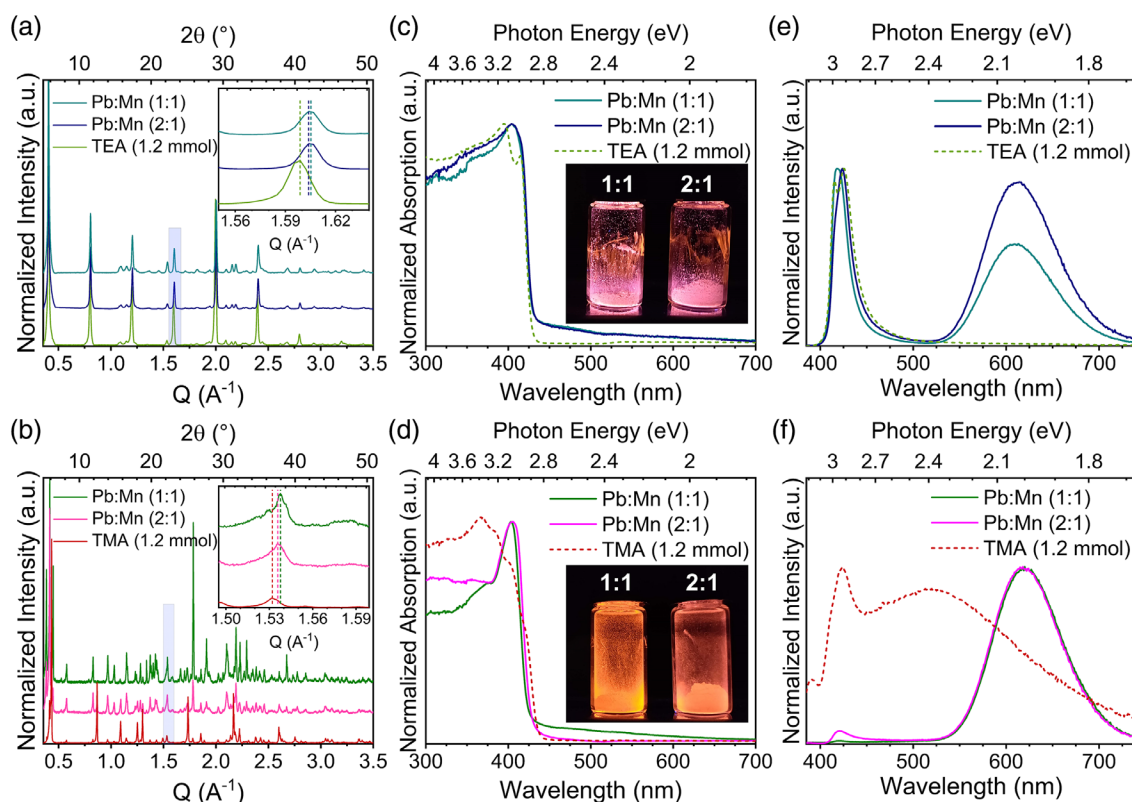


Figure 5. a,b) Powder XRD pattern collected from the a) Mn-doped TEA- and b) TMA-based crystals. The insets display a magnified view of the region highlighted in blue and show the shift toward a higher 2θ of the diffraction peaks with respect to the undoped samples. c,d) Absorption and e,f) emission spectra of the samples. The insets in (c) and (d) show photographs of the dried crystals under UV light.

a contraction in the in-plane lattice parameters. This is associated with the replacement of the large Pb^{2+} ions with smaller Mn^{2+} ions in the structure rather than the interstitial position, which causes an expansion of the lattice.

The absorption spectra of the doped samples in Figure 5c-d show similar characteristics as the undoped ones. The emission spectra of TMA-based samples display predominantly the Mn-related emission peak, with only weak blue band edge emission (Figure 5f). The blue emission is slightly evident in the samples with the 2:1 ratio and it is completely suppressed in the samples prepared with an equimolar ratio (1:1) of Mn and Pb precursors. We find a much higher percentage of Mn^{2+} substitution in the 2D HLP lattice of the 1:1 sample, with respect to the 2:1 one, as determined by the ICP analysis. Intriguingly, the Mn-doped TEA-based samples (Figure 5e) show both the band-to-band emission of 2D HLPs and the largely Stokes-shifted broader emission at 610 nm that arises from the Mn^{2+} d-d transitions.^[36,38] The perceived color of the Mn-doped samples can be significantly modified by the choice of amine and Mn concentration in the orange-to-red range (insets of Figure 5c,d and corresponding color coordinates in Figure S8 and Table S5, Supporting Information). In particular, the intensity ratio of the blue band edge emission to the Mn-related red emission peak can be largely varied for the TEA samples, where, for a 2:1 ratio of Pb and Mn, similar peak amplitudes are obtained. The photoluminescence quantum yield (PLQY) of the Mn-doped samples reaches $\approx 20\%$ on the TMA (1:1) ratio (Table S5, Supporting Information). These results open new avenues for designing the perceived emission color from single 2D-layered materials.

3. Conclusion

In summary, we have synthesized 2D-layered lead bromide perovskites with a Ruddlesden–Popper phase using conjugated cations and shown that the emission of these structures can be tuned from blue to white by changing the organic cation and HBr precursor concentration in the synthesis. Furthermore, we demonstrated reversible switching of the emission color by activating or suppressing the broad emission peak in the green-to-red visible spectrum via simple solution treatments. Mn^{2+} doping of these thiophene-based 2D HLPs ultimately enlarged the color tunability to the orange–red spectral range. The color tunability and reversible color changes of a single material that we demonstrate here can be expected to strongly stimulate the development of light emission devices, where color rendering is desired, and open pathways for applications where active switching of optical emission is essential.

4. Experimental Section

Materials: PbBr_2 (98%), hydrobromic acid (HBr, 47% m/m in water), 2-thiophenemethylamine (96%), and 2-thiopheneethylamine (96%) were purchased from Sigma-Aldrich. All the chemicals were used without further purification.

Synthesis of 2D HLP Crystals: For the 0.6 mmol samples, stoichiometric amounts of PbBr_2 powder (110 mg, 0.3 mmol) were dissolved in 0.07 mL

of HBr (0.6 mmol) in a vial and 1 mL of acetone was added under vigorous shaking. For the 1.2 mmol samples, PbBr_2 (110 mg, 0.3 mmol) powders were dissolved in 0.14 mL of HBr (1.2 mmol) and acetone or toluene was used as a solvent for TMA samples. The resulting solutions were clear and transparent. Next, the selected thiophene was injected to the mixtures under strong magnetic stirring and two different concentrations were used: 0.6 and 1.2 mmol for each type of amine. The vials were left overnight under shaking and the collected crystals were washed in acetone to remove the unreacted precursors. Finally, the crystals were centrifuged at 5500 RPM for 5 min and dried under the hood.

Post-Treatment of 2D HLP Crystals: Post-treatment of TMA-based crystals was conducted by immersing the crystals in 1 mL of acetone along with 140 μL (1.2 mmol) of HBr and 123 μL (1.2 mmol) of TMA. The vials were left overnight under shaking for the complete reaction. The crystals were collected after centrifugation at 5500 RPM for 5 min and dried under the hood for further studies.

Synthesis of Mn-doped 2D HLP Crystals: For the preparation of the (1:1) samples, an equimolar ratio of PbBr_2 (55 mg, 0.15 mmol) and MnBr_2 (32 mg, 0.15 mmol) powders was dissolved in 140 μL (1.2 mmol) of HBr solution and 1 mL of acetone under vigorous shaking, forming a clear and transparent solution. Then, the selected amine (1.2 mmol) was injected into the mixture under strong magnetic stirring and left overnight for the complete reaction. The crystals were centrifuged at 5500 RPM for 5 min to remove the unreacted precursors. Finally, the samples were annealed at 90° for 3 h in an oven and ground using mortar and pestle to promote the incorporation of more Mn ions into the structure. The (2:1) samples were prepared by adding 0.3 mmol (110 mg) of PbBr_2 powder along with 0.15 mmol (32 mg) of MnBr_2 powder in HBr and acetone following the same protocol. Elemental analysis of the Mn-doped 2D HLPs was conducted via inductively coupled optical emission spectroscopy using a Thermo Fisher iCAP 6300 duo instrument. Few mg of each sample were digested overnight in a mixture of nitric acid and HCl ($\text{HNO}_3 + \text{HCl}$ in 3:1 volume ratio) solution (2.5 mL) and diluted in Milli-Q water for a total volume of 25 mL. All the suspensions were filtered before analysis using polytetrafluoroethylene (PTFE) filters.

Structural and Morphological Characterization: SEM analysis on the resulting 2D-layered halide perovskites was conducted on an FEI Nova 600 NanoLab instrument by depositing the dried crystals directly on Si substrates. XRD studies were conducted on finely grounded samples on a PANalytical Empyrean X-ray diffractometer equipped with a Cu K α ceramic X-ray tube (operated at 45 kV and 40 mA) and PIXcel^{3D} 2 \times 2 area detector. Diffraction patterns with higher resolution were obtained using a Rigaku SmartLab system, equipped with a 9 kW rotating Cu anode working at 40 kV and 150 mA and a D/teX Ultra 1D silicon strip detector. The samples were grounded using an agate mortar and deposited on zero-diffraction Si substrates.

Optical Characterization: The absorption spectra were collected from the dried crystals using a Varian Cary 5000 ultraviolet–visible–near-infrared (UV–vis–NIR) spectrophotometer equipped with an external diffuse reflectance accessory and operating in absorption geometry. The PL, PLE spectra, and PLQE measurements were carried out on an Edinburgh Instruments (FLS920) fluorescence spectrometer equipped with a Xenon-lamp with a monochromator for steady-state PLE. The PL spectra were collected with an excitation wavelength of 375 nm. The PL and PLE spectra were collected with 1 nm resolution and 0.5 s of dwell time. The PLQE values were obtained from three different samples from different syntheses batches by exciting them at 375 nm using a calibrated integrating sphere with step increments of 1 nm and integration time of 0.2 s per data point for five repetition cycles. Light absorption due to scattering inside the sphere was taken into account for the PLQE calculation by collecting three different spectra: 1) directly exciting the sample in the sphere, 2) indirectly exciting sample in the sphere, and 3) without the sample in the sphere. Time-resolved PL measurements were carried out with a time-correlated single-photon counting (TCSPC) unit coupled to a pulsed diode laser. The samples were excited at 375 nm with picosecond pulses at a repetition rate of 1 MHz, and the signal was collected with a spectral window of 10 nm. The samples were placed in between two clean glass substrate for all these studies.

Commission Internationale de l'Éclairage (CIE) coordinates, CRI, and correlated colour temperature (CCT) values were obtained from Colour Calculator by OSRAM Sylvania, Inc.

Supporting Information

Supporting Information is available from the Wiley Online Library or from the author.

Acknowledgements

M.A. and B.D. thank S. Lauciello from the Electron Microscopy Facility, F. Drago from the Nanochemistry Facility, and Dr. M. Prato from the Materials Characterization Facility at the Istituto Italiano di Tecnologia for their technical support and discussions on the chemical compositions of the doped samples. This work received funding from the AI-4-QD project financed by the Italian Ministry of Foreign Affairs and International Cooperation (MAECI) within the bilateral Italy–Israel program.

Conflict of Interest

The authors declare no conflict of interest.

Data Availability Statement

Research data are not shared.

Keywords

conjugated molecules, emission tunability, layered perovskites, structural defects, thiophenes, white emission

Received: January 11, 2021

Revised: February 12, 2021

Published online:

- [1] Y. Gao, E. Shi, S. Deng, S. B. Shiring, J. M. Snaider, C. Liang, B. Yuan, R. Song, S. M. Janke, A. Liebman-Peláez, P. Yoo, M. Zeller, B. W. Boudouris, P. Liao, C. Zhu, V. Blum, Y. Yu, B. M. Savoie, L. Huang, L. Dou, *Nat. Chem.* **2019**, *11*, 1151.
- [2] a) M. D. Smith, B. A. Connor, H. I. Karunadasa, *Chem. Rev.* **2019**, *119*, 3104; b) J. Di, J. Chang, S. Liu, *EcoMat* **2020**, *2*, e12036; c) F. Zhang, H. Lu, J. Tong, J. J. Berry, M. C. Beard, K. Zhu, *Energy Environ. Sci.* **2020**, *13*, 1154.
- [3] a) H. Ren, S. Yu, L. Chao, Y. Xia, Y. Sun, S. Zuo, F. Li, T. Niu, Y. Yang, H. Ju, B. Li, H. Du, X. Gao, J. Zhang, J. Wang, L. Zhang, Y. Chen, W. Huang, *Nat. Photonics* **2020**, *14*, 154; b) B. Sun, Y. Xu, Y. Chen, W. Huang, *APL Mater.* **2020**, *8*, 040901.
- [4] Y. Chen, Y. Sun, J. Peng, J. Tang, K. Zheng, Z. Liang, *Adv. Mater.* **2018**, *30*, 1703487.
- [5] a) P. Huang, S. Kazim, M. Wang, S. Ahmad, *ACS Energy Lett.* **2019**, *4*, 2960; b) D. Ghosh, D. Acharya, L. Pedesseau, C. Katan, J. Even, S. Tretiak, A. J. Neukirch, *J. Mater. Chem. A* **2020**, *8*, 22009.
- [6] a) I. Spanopoulos, I. Hadar, W. Ke, Q. Tu, M. Chen, H. Tsai, Y. He, G. Shekhawat, V. P. Dravid, M. R. Wasielewski, A. D. Mohite, C. C. Stoumpos, M. G. Kanatzidis, *J. Am. Chem. Soc.* **2019**, *141*, 5518; b) I. C. Smith, E. T. Hoke, D. Solis-Ibarra, M. D. McGehee, H. I. Karunadasa, *Angew. Chem. Int. Ed.* **2014**, *53*, 11232.
- [7] a) G. Grancini, C. Roldán-Carmona, I. Zimmermann, E. Mosconi, X. Lee, D. Martineau, S. Narbey, F. Oswald, F. De Angelis, M. Graetzel, M. K. Nazeeruddin, *Nat. Commun.* **2017**, *8*, 15684; b) Z. Wang, Q. Lin, F. P. Chmiel, N. Sakai, L. M. Herz, H. J. Snaith, *Nat. Energy* **2017**, *2*, 17135; c) P. Li, Y. Zhang, C. Liang, G. Xing, X. Liu, F. Li, X. Liu, X. Hu, G. Shao, Y. Song, *Adv. Mater.* **2018**, *30*, 1805323.
- [8] a) J. C. Blancon, A. V. Stier, H. Tsai, W. Nie, C. C. Stoumpos, B. Traoré, L. Pedesseau, M. Kepenekian, F. Katsutani, G. T. Noe, J. Kono, S. Tretiak, S. A. Crooker, C. Katan, M. G. Kanatzidis, J. J. Crochet, J. Even, A. D. Mohite, *Nat. Commun.* **2018**, *9*, 2254; b) X. Hong, T. Ishihara, A. V. Nurmikko, *Phys. Rev. B* **1992**, *45*, 6961; c) B. Cheng, T.-Y. Li, P. Maity, P.-C. Wei, D. Nordlund, K.-T. Ho, D.-H. Lien, C.-H. Lin, R.-Z. Liang, X. Miao, I. A. Ajia, J. Yin, D. Sokaras, A. Javey, I. S. Roqan, O. F. Mohammed, J.-H. He, *Commun. Phys.* **2018**, *1*, 80.
- [9] a) J. Ma, C. Fang, C. Chen, L. Jin, J. Wang, S. Wang, J. Tang, D. Li, *ACS Nano* **2019**, *13*, 3659; b) G. Long, R. Sabatini, M. I. Saidaminov, G. Lakhwani, A. Rasmata, X. Liu, E. H. Sargent, W. Gao, *Nat. Rev. Mater.* **2020**, *5*, 423.
- [10] B. Dhanabalan, A. Castelli, M. Palei, D. Spirito, L. Manna, R. Krahn, M. Arciniegas, *Nanoscale* **2019**, *11*, 8334.
- [11] a) Z. Yuan, Y. Shu, Y. Tian, Y. Xin, B. Ma, *Chem. Commun.* **2015**, *51*, 16385; b) R. Dong, C. Lan, X. Xu, X. Liang, X. Hu, D. Li, Z. Zhou, L. Shu, S. Yip, C. Li, S.-W. Tsang, J. C. Ho, *ACS Appl. Mater. Interfaces* **2018**, *10*, 19019.
- [12] a) E. R. Dohner, E. T. Hoke, H. I. Karunadasa, *J. Am. Chem. Soc.* **2014**, *136*, 1718; b) C. Ji, S. Wang, L. Li, Z. Sun, M. Hong, J. Luo, *Adv. Funct. Mater.* **2019**, *29*, 1805038.
- [13] E. R. Dohner, A. Jaffe, L. R. Bradshaw, H. I. Karunadasa, *J. Am. Chem. Soc.* **2014**, *136*, 13154.
- [14] H. Lin, C. Zhou, Y. Tian, T. Siegrist, B. Ma, *ACS Energy Lett.* **2018**, *3*, 54.
- [15] S. Yang, Z. Lin, J. Wang, Y. Chen, Z. Liu, E. Yang, J. Zhang, Q. Ling, *ACS Appl. Mater. Interfaces* **2018**, *10*, 15980.
- [16] M. D. Smith, H. I. Karunadasa, *Acc. Chem. Res.* **2018**, *51*, 619.
- [17] J. Yin, R. Naphade, L. Gutiérrez Arzaluz, J.-L. Brédas, O. M. Bakr, O. F. Mohammed, *ACS Energy Lett.* **2020**, *5*, 2149.
- [18] D. Y. Park, S.-J. An, C. Lee, D. A. Nguyen, K.-N. Lee, M. S. Jeong, *J. Phys. Chem. Lett.* **2019**, *10*, 7942.
- [19] a) L. Dou, A. B. Wong, Y. Yu, M. Lai, N. Kornienko, S. W. Eaton, A. Fu, C. G. Bischak, J. Ma, T. Ding, N. S. Ginsberg, L.-W. Wang, A. P. Alivisatos, P. Yang, *Science* **2015**, *349*, 1518; b) S. Yang, W. Niu, A.-L. Wang, Z. Fan, B. Chen, C. Tan, Q. Lu, H. Zhang, *Angew. Chem. Int. Ed.* **2017**, *56*, 4252; c) I. Neogi, A. Bruno, D. Bahulayan, T. W. Goh, B. Ghosh, R. Ganguly, D. Cortecchia, T. C. Sum, C. Soci, N. Mathews, S. G. Mhaisalkar, *ChemSusChem* **2017**, *10*, 3765; d) A. Yangui, D. Garrot, J. S. Lauret, A. Lussan, G. Bouchez, E. Deleporte, S. Pillet, E. E. Bendeif, M. Castro, S. Triki, Y. Abid, K. Boukheddaden, *J. Phys. Chem. C* **2015**, *119*, 23638; e) B. Febriansyah, D. Giovanni, S. Ramesh, T. M. Koh, Y. Li, T. C. Sum, N. Mathews, J. England, *J. Mater. Chem. C* **2020**, *8*, 889.
- [20] D. Cortecchia, S. Neutzner, A. R. Srimath Kandada, E. Mosconi, D. Meggiolaro, F. De Angelis, C. Soci, A. Petrozza, *J. Am. Chem. Soc.* **2017**, *139*, 39.
- [21] Y. Y. Li, C. K. Lin, G. L. Zheng, Z. Y. Cheng, H. You, W. D. Wang, J. Lin, *Chem. Mater.* **2006**, *18*, 3463.
- [22] Y. Li, G. Zheng, J. Lin, *Eur. J. Inorg. Chem.* **2008**, *2008*, 1689.
- [23] L. Mao, Y. Wu, C. C. Stoumpos, M. R. Wasielewski, M. G. Kanatzidis, *J. Am. Chem. Soc.* **2017**, *139*, 5210.

- [24] a) M. D. Smith, A. Jaffe, E. R. Dohner, A. M. Lindenberg, H. I. Karunadasa, *Chem. Sci. J.* **2017**, *8*, 4497; b) Y. Han, Y. Li, Y. Wang, G. Cao, S. Yue, L. Zhang, B.-B. Cui, Q. Chen, *Adv. Opt. Mater.* **2020**, *8*, 1902051.
- [25] C. Ni, Y. Huang, T. Zeng, D. Chen, H. Chen, M. Wei, A. Johnston, A. H. Proppe, Z. Ning, E. H. Sargent, P. Hu, Z. Yang, *Angew. Chem. Int. Ed.* **2020**, *59*, 13977.
- [26] Z. Yuan, C. Zhou, Y. Tian, Y. Shu, J. Messier, J. C. Wang, L. J. van de Burgt, K. Kountouriotis, Y. Xin, E. Holt, K. Schanze, R. Clark, T. Siegrist, B. Ma, *Nat. Commun.* **2017**, *8*, 14051.
- [27] Palmer, D. C., CrystalMaker, CrystalMaker Software Ltd. Begbroke, Oxfordshire, UK **2014**.
- [28] X. Gong, O. Voznyy, A. Jain, W. Liu, R. Sabatini, Z. Piontkowski, G. Walters, G. Bappi, S. Nokhrin, O. Bushuyev, M. Yuan, R. Comin, D. McCamant, S. O. Kelley, E. H. Sargent, *Nat. Mater.* **2018**, *17*, 550.
- [29] A. Castelli, G. Biffi, L. Ceseracciu, D. Spirito, M. Prato, D. Altamura, C. Giannini, S. Artyukhin, R. Krahne, L. Manna, M. P. Arciniegas, *Adv. Mater.* **2019**, *31*, 1805608.
- [30] a) M. D. Smith, B. L. Watson, R. H. Dauskardt, H. I. Karunadasa, *Chem. Mater.* **2017**, *29*, 7083; b) S. Bhaumik, A. Bruno, S. Mhaisalkar, *RSC Adv.* **2020**, *10*, 13431.
- [31] B. Dhanabalan, G. Biffi, A. Moliterni, V. Olieric, C. Giannini, G. Saleh, L. Ponet, M. Prato, I. Muhammad, L. Manna, R. Krahne, S. Artyukhin, M. P. Arciniegas, *Adv. Mater.* **2021**, 2008004.
- [32] Q. Zhang, Y. Ji, Z. Chen, D. Vella, X. Wang, Q.-H. Xu, Y. Li, G. Eda, *J. Phys. Chem. Lett.* **2019**, *10*, 2869.
- [33] a) B. Febriansyah, T. Borzda, D. Cortecchia, S. Neutzner, G. Folpini, T. M. Koh, Y. Li, N. Mathews, A. Petrozza, J. England, *Angew. Chem. Int. Ed.* **2020**, *59*, 10791; b) Z. Yuan, C. Zhou, J. Messier, Y. Tian, Y. Shu, J. Wang, Y. Xin, B. Ma, *Adv. Opt. Mater.* **2016**, *4*, 2009; c) H. Hu, S. A. Morris, X. Qiao, D. Zhao, T. Salim, B. Chen, E. E. M. Chia, Y. M. Lam, *J. Mater. Chem. C* **2018**, *6*, 10301.
- [34] J. M. Hoffman, X. Che, S. Sidhik, X. Li, I. Hadar, J.-C. Blancon, H. Yamaguchi, M. Kepenekian, C. Katan, J. Even, C. C. Stoumpos, A. D. Mohite, M. G. Kanatzidis, *J. Am. Chem. Soc.* **2019**, *141*, 10661.
- [35] a) M. Abdi-Jalebi, M. Pazoki, B. Philippe, M. I. Dar, M. Alsari, A. Sadhanala, G. Divitini, R. Imani, S. Lilliu, J. Kullgren, H. Rensmo, M. Grätzel, R. H. Friend, *ACS Nano* **2018**, *12*, 7301; b) D.-Y. Son, S.-G. Kim, J.-Y. Seo, S.-H. Lee, H. Shin, D. Lee, N.-G. Park, *J. Am. Chem. Soc.* **2018**, *140*, 1358.
- [36] A. K. Guria, S. K. Dutta, S. D. Adhikari, N. Pradhan, *ACS Energy Lett.* **2017**, *2*, 1014.
- [37] a) D. Bai, J. Zhang, Z. Jin, H. Bian, K. Wang, H. Wang, L. Liang, Q. Wang, S. F. Liu, *ACS Energy Lett.* **2018**, *3*, 970; b) T. Sheikh, A. Nag, *J. Phys. Chem. C* **2019**, *123*, 9420; c) W. J. Mir, A. Swarnkar, A. Nag, *Nanoscale* **2019**, *11*, 4278.
- [38] Q. Ba, A. Jana, L. Wang, K. S. Kim, *Adv. Funct. Mater.* **2019**, *29*, 1904768.